THE JOURNAL OF BIOLOGICAL CHEMISTRY VOL. 288, NO. 51, pp. 36624–36635, December 20, 2013
Published in the U.S.A.

Altered Intersubunit Communication Is the Molecular Basis for Functional Defects of Pathogenic p97 Mutants*

Received for publication, May 30, 2013, and in revised form, October 21, 2013 Published, JBC Papers in Press, November 6, 2013, DOI 10.1074/jbc.M113.488924

Wai Kwan Tang and Di Xia[1]
From the Laboratory of Cell Biology, Center for Cancer Research, NCI, National Institutes of Health, Bethesda, Maryland 20892

Background: Single-point mutations in AAA chaperone p97 cause multiple disorders, but the molecular basis remains unknown.
Results: Significant differences in structural and biochemical properties between wild type and pathogenic p97 were revealed.
Conclusion: Mutations altered the communication among subunits within a hexameric p97, resulting in p97 molecules with defective function.
Significance: Mechanistic insights into the function of p97 are provided.

The human AAA ATPase p97 is a molecular chaperone essential in cellular proteostasis. Single amino acid substitutions in p97 have been linked to a clinical multiple-disorder condition known as inclusion body myopathy associated with Paget's disease of the bone and frontotemporal dementia. How the mutations affect the molecular mechanism that governs the function of p97 remains unclear. Here, we show that within the hexameric ring of a mutant p97, D1 domains fail to regulate their respective nucleotide-binding states, as evidenced by the lower amount of prebound ADP, weaker ADP binding affinity, full occupancy of adenosine-5′-O-(3-thiotriphosphate) binding, and elevated overall ATPase activity, indicating a loss of communication among subunits. Defective communication between subunits is further illustrated by altered conformation in the side chain of residue Phe-360 that probes into the nucleotide-binding pocket from a neighboring subunit. Consequently, conformations of N domains in a hexameric ring of a mutant p97 become uncoordinated, thus impacting its ability to process substrate.

Inclusion body myopathy associated with Paget disease of the bone and frontotemporal dementia (IBMPFD)[2] is a late-onset multiple disorder that mainly affects three tissue types: muscle, bone, and brain. The disease is attributed to missense mutations in the p97 gene (1). Although diverse single-amino acid changes in IBMPFD patients at 14 positions of the primary sequence of p97 have been identified (2–4), no clear correlation has been found between the site/type of mutations and clinical manifestations of the disease; individuals having the same mutation can exhibit different symptoms. Nevertheless, a common pathology found in patient muscle and brain tissues is the accumulation of cytoplasmic proteinous inclusions (1, 5), suggesting cellular deficiency in removing unwanted proteins. Progress has been made in *in vitro* studies using cultured cells expressing IBMPFD p97 mutants, revealing impairment in various protein degradation pathways, including endoplasmic reticulum-associated degradation (6), autophagy (7–9), and sorting of ubiquitylated cargo in the endocytic pathway (10). However, questions remain concerning the role of p97 in these pathways and the effects of IBMPFD mutations on the molecular function of p97.

Human p97, also called valosin-containing protein (VCP), is a homohexameric ATPase and a member of the Type II AAA (ATPases associated with various cellular activities) protein family. Each subunit or protomer of p97 is composed of three main domains: an N-terminal domain (N domain) and two AAA ATPase domains, D1 and D2 (11, 12) (Fig. 1*A*). Structurally, the D1- and D2 domains form two concentric, stacked rings. Whereas D1 domains are responsible for the homohexamerization regardless of their nucleotide states, D2 domains are attributed to the majority of ATP hydrolyzed by p97. The N domains are attached peripherally to the D1 ring and move considerably during the ATP hydrolysis cycle, as shown by multiple conformations modeled from low resolution electron microscopy (13) and small angle x-ray scattering studies in the presence of different nucleotides (14, 15). Because N domains are largely responsible for interacting with various adaptor proteins, their conformational flexibilities are believed to be critical for p97 to properly handle substrates that bind to adaptor proteins. Despite the apparent flexibility of the N domains observed using low resolution techniques, high resolution crystal structures of wild type p97 always show ADP bound at the D1 domain with the N domains in a single conformation attaching to the side of and co-planar with the D1 ring (down-conformation) (11, 12, 16, 18). Only in a crystallographic study of IBMPFD mutants was a nucleotide-dependent N domain conformational change of p97 observed, in which an up-conformation (when the N domains rise above the D1 ring) and a

* This work was supported, in whole or in part, by the National Institutes of Health Intramural Research Program (NCI, Center for Cancer Research).
The atomic coordinates and structure factors (codes 4KLN, 4KO8, and 4KOD) have been deposited in the Protein Data Bank (http://wwpdb.org/).
[1] To whom correspondence should be addressed: Laboratory of Cell Biology, NCI, National Institutes of Health, 37 Convent Dr., Bldg. 37, Rm. 2122C, Bethesda, MD 20892. Tel.: 301-435-6315; Fax: 301-480-2315; E-mail: xiad@mail.nih.gov.
[2] The abbreviations used are: IBMPFD, inclusion body myopathy associated with Paget disease of the bone and frontotemporal dementia; AAA, ATPases associated with various cellular activities; ATPγS, adenosine-5′-*O*-(3-thiotriphosphate); ITC, isothermal titration calorimetry; SRH, second region of homology; VCP, valosin-containing protein; PDB, Protein Data Bank.

This is an Open Access article under the CC BY license.

down-conformation were demonstrated in the presence of ATPγS and ADP, respectively (15) (Fig. 1*B*).

IBMPFD mutations in p97 are found at neither the nucleotide-binding sites nor any known adaptor protein-binding interface that would have predicted a direct adverse effect on the function of p97. Instead, they cluster at the interface between the N and the D1 domain (15). These pathogenic mutants are able to form proper hexamers just like the wild type (6, 15, 19, 20) and do not introduce apparent alterations to the part of the structure where they occur (15). Thus, the structural differences between pathogenic mutants and the wild type p97 is rather subtle. Indeed, biochemical and biophysical characterizations of a couple of mutants demonstrated lowered ADP-binding affinities toward the D1 domain and exhibited biphasic exothermal profiles when they were titrated with ATPγS (15). It is conceivable that such deviations in the nucleotide-binding properties of mutant p97 may also be reflected in their ATPase activities. However, conflicting observations have been reported showing that the pathogenic p97 mutants have either similar (6, 21) or higher (19, 20, 22) ATPase activities compared with the wild type.

Although synergistic coupling or communication has been suggested to exist among cognate domains and between different subunits of p97 and other AAA proteins (14, 23–29), characterization of these interactions in wild type p97 remains challenging and has not been investigated in pathogenic p97. Therefore, if confirmed, the alteration of ATPase activities by IBMPFD mutations would constitute a clear demonstration of communication among different domains of p97. More significantly, study of this phenomenon will not only lead us to an understanding of the effect of IBMPFD mutations on p97 function but also provide a means to investigate the interactions between domains from the same subunit or between different subunits. In the present study, we report observable deviations in a number of biochemical, biophysical, and structural properties that set IBMPFD mutants apart from wild type p97. These include differences in the amount of prebound ADP at the D1 site, changes in ADP-binding affinity at the D1 domain, alterations in ATPase activity, and changes in structure of the protein at the D1 nucleotide-binding pocket. These differences point to an altered regulation of the nucleotide states of the D1 domain in pathogenic p97, which may affect the downstream handling of substrates by the protein.

EXPERIMENTAL PROCEDURES

Mutagenesis and Protein Purification—Expression plasmids pQE60-p97 and pQE60-p97N-D1 were constructed as previously described to overexpress p97 proteins in a bacterial system (15). All mutations and truncates were generated using a QuikChange® site-directed mutagenesis kit (Agilent Technologies, Santa Clara, CA). Proteins were expressed in the *Escherichia coli* strain M15 (Qiagen, Valencia, CA) at 37 °C. Cell lysate was incubated with nickel-nitrilotriacetic acid resin (Qiagen, Valencia, CA) at 4 °C for 30 min and washed, and p97 was eluted with 250 mM imidazole in a buffer containing 25 mM Tris-HCl, pH 7.5, 300 mM NaCl, and 10% glycerol. Fractions containing p97 were concentrated and then dialyzed against 20 mM Tris-HCl, pH 8.0, 10% glycerol and stored at −80 °C.

Identification and Quantification of Prebound Nucleotide—Protein samples were dialyzed extensively against Buffer A (50 mM Tris-HCl, pH 8.0, 2 mM $MgCl_2$) for 16 h at 4 °C before use. A total of 500 μg of protein in Buffer A was heated at 95 °C for 10 min. Precipitate was removed by passing through a 0.22-μm spin filter (Millipore, Billerica, MA). Filtrate was then loaded directly onto a MonoQ HR 5/5 column (GE Healthcare) pre-equilibrated with Buffer A. Elution was done by an NaCl gradient (0–1 M) in Buffer A and was monitored by UV absorbance at 260 nm. The amount of nucleotide in the samples was determined from the peak area in reference to an ADP standard curve. The ADP standard curve was generated by injecting a known amount of ADP (0.00125–0.02 μmol) into the MonoQ column, which was eluted using the same elution protocol as mentioned above. The molar ratio between ADP and p97 monomer was then calculated. Protein concentration was determined by spectrophotometric measurement at 280 nm using a calculated molar extinction coefficient of 21,430 M^{-1} cm^{-1}.

Removal of Prebound ADP by Apyrase Treatment—One microliter of 1 mg/ml apyrase (an isoform with low ATPase/ADPase ratio) (Sigma-Aldrich) was mixed with ~5 mg of p97 protein in storage buffer and incubated at 4 °C for 16 h. The p97 sample was then repurified by running through Superdex™ 200 (GE Healthcare) pre-equilibrated with 50 mM Tris-HCl, pH 8.0, 2 mM $MgCl_2$, and 5% glycerol. An aliquot of the sample was taken out to determine the amount of prebound nucleotide using the method described above.

Measurement of Nucleotide-binding Affinity by Isothermal Titration Calorimetry (ITC)—ITC experiments were performed using a VP-ITC titration microcalorimeter (GE Healthcare). Protein samples were dialyzed against 50 mM Tris-HCl, pH 8.0, 2 mM $MgCl_2$, and 5% glycerol at 4 °C overnight, and the same buffer was used to prepare the nucleotides. All titrations were performed in the buffer at 25 °C. Data were fitted using the one-type of site model or two-type of site model from Origin® version 7.0 software (OriginLab, Northampton, MA).

Measurement of ATPase Activity—ATPase activity of p97 was determined by measuring the amount of inorganic phosphate released from ATP hydrolysis, which reacts with molybdate and malachite green (30, 31). The activity assay was performed in buffer containing 50 mM Tris-HCl, pH 8.0, 20 mM $MgCl_2$, 1 mM EDTA, and 1 mM DTT. A total of 50 μl of reaction mix containing 2–5 μg of protein and 4 mM buffered ATP was incubated at 37 °C for 15 min. The reaction was immediately stopped by the addition of 800 μl of dye buffer (a fresh mixture of 0.045% malachite green and 1.4% ammonium molybdate tetrahydrate in 4 N HCl in a 1:3 ratio) followed by the addition of 100 μl of 34% sodium citrate solution after 1 min. After a 10-min incubation at room temperature, 16 μl of 10% Tween 20 was added to dissolve any precipitate. Absorbance was then measured at 660 nm. The amount of inorganic phosphate released was calculated based on the standard curve established by a known amount of KH_2PO_4 (10–100 μM) in assay buffer.

Crystallization and X-ray Diffraction Data Collection—Crystals of the p97 N-D1 truncate bearing the A232E mutation were obtained by the sitting drop vapor diffusion method at 21 °C. Proteins were first treated with $MgCl_2$ and nucleotide ATPγS at a final concentration of 40 and 4 mM, respectively, for

30 min at 4 °C. The admixture was centrifuged at 12,600 × *g* for 30 min, and the supernatant was used for crystallization. Crystals with bound ATPγS were grown by mixing 2 μl of the protein solution with 2 μl of precipitant solution (0.1 M sodium citrate, pH 5.8, 0.3 M NaCl, 9% PEG 3350, 13% glycerol, and 2% benzamidine). Crystals with bound ATPγS were cryoprotected by stepwise soaking in buffer solutions containing 10 mM Tris-HCl, pH 8, 2% benzamidine, 50 mM sodium citrate, pH 5.8, 20 mM $MgCl_2$ with increasing amounts of glycerol and PEG 3350 to a final concentration of 28 and 20%, respectively. The crystals were flash-frozen in liquid propane. Crystals for the R155H mutant were obtained in a manner similar to that described previously (32).

X-ray diffraction experiments were carried out at 100 K at the SER-CAT beam line of the Advanced Photon Source at Argonne National Laboratory. Diffraction images were collected with MarCCD detectors and processed and scaled with the HKL2000 package (33).

Structure Determination—The structures of the A232E mutant bound with ATPγS were determined by molecular replacement with the program Phaser (34) using PDB entry 3HU3 (15) as a search model. The structures were refined using Refmac (35) in the CCP4 program package (36). All structure models were manually manipulated using the program COOT (37).

RESULTS

Mutations at 14 positions in the primary sequence of p97 have been identified in patients diagnosed with IBMPFD. Most of these mutations were found at the N domain, and some localized at the D1 domain or the N-D1 linker region, but none were found in the D2 domain. Among them, the mutation at residue Arg-155 occurs most frequently. Previously, we reported biophysical and structural studies on two N-D1 fragments of p97 bearing IBMPFD mutations (R95G or R155H) in the N domain, which revealed their reduced ADP binding affinities to the D1 domain and nucleotide-dependent conformational change of the N domain (15). It is of great interest to investigate whether these altered properties identified for the N domain mutants can be extended to mutations in other parts of p97, especially in the D1 domain. Here, by using six IBMPFD mutants (two each from the N domain (R95G and R155H), the N-D1 linker region (R191Q and L198W), and the D1 domain (A232E and T262A) (Fig. 1*A*)), not only did we confirm previous results for all mutants, but we were able to identify additional properties that deviate from the wild type. As we shall see, all of these observed deviations reveal an altered communication pathway in pathogenic p97, which affects the cellular functions of p97 and leads to the disease.

IBMPFD Mutants Invariably Have a Reduced Amount of Prebound ADP at the D1 Site—Earlier studies on wild type p97 showed that a significant portion (50–90%) of the D1 domain is occupied by ADP that is very difficult to remove (14, 38). By ITC measurements, we consistently observed that the titration stoichiometry (*N*) for ADP in all N-D1 truncates of p97 possessing IBMPFD mutations was substantially higher than that in the wild type N-D1 (Table 1), suggesting a smaller amount of ADP retained in preparations of the purified mutant proteins. Because the ADP titration stoichiometry measured by ITC does not directly demonstrate the presence of prebound ADP and is dependent on accurate determination of active enzyme concentration, we sought a direct method to ascertain the amount of prebound nucleotide. Purified N-D1 p97 mutant proteins were heat-denatured to release any bound nucleotide, followed by ion-exchange chromatography to determine the type and quantity of the nucleotide. Elution peaks appearing at the same chromatographic position as that of the ADP standard were observed in all samples, confirming that the identity of prebound nucleotide is ADP. Integration of peak absorbance revealed that, in the wild type protein, about 53% of the D1 sites had ADP bound, whereas a significantly lower amount of prebound ADP, ranging from ~11 to 36%, was present at the D1 sites of the IBMPFD mutants (Fig. 2*A*). The lower amounts of prebound ADP, which leave more empty D1 sites available for ADP titration, correlate inversely with the higher titration stoichiometries observed for these mutants in the ITC experiments (Fig. 2*A* and Table 1).

Mutants Have an Altered Binding Affinity for ADP but Not ATP at the D1 Site—Regardless of the locations of the mutations, all N-D1 truncates showed weaker ADP binding when compared with the wild type (Fig. 2*B* and Table 1), which is in accordance with the reduced amount of prebound ADP. The reduction in the affinity does not appear to correlate directly with the nature of the mutation (charge, size, or location). Among all mutants tested, R155H and A232E exhibited the lowest ADP binding affinity, with K_d values of 4.25 and 5.15 μM, respectively.

Previously, titration of ATPγS to N-D1 IBMPFD mutants (R155H and R95G) by ITC yielded a biphasic binding isotherm, which can only be fitted by a two-site model *versus* the monotonic binding isotherm observed in wild type N-D1 (15). In an earlier publication (39), we proposed that this profile could serve as a molecular hallmark for IBMPFD mutants. In the present study, this biphasic binding signature was seen for all of the mutants tested (Fig. 3*A*). Because IBMPFD mutants showed a significant reduction in prebound ADP and a lowered ADP binding affinity, we reasoned that the biphasic titration profile could reflect ATPγS binding to two types of D1 sites: the empty sites and sites with prebound ADP. To test this hypothesis, we treated the N-D1 mutant proteins with apyrase to remove any prebound ADP and confirmed that no residual nucleotide remained by the heat denaturation procedure described above. We then used ITC to measure ATPγS binding with the apyrase-treated samples. As predicted, the binding isotherms for ATPγS were no longer biphasic (Fig. 3*B*), and the binding stoichiometries were close to unity for both wild type and mutant N-D1 p97, indicating nearly complete elimination of prebound ADP (Table 2). The ADP-free forms of both wild type and IBMPFD mutants of N-D1 had similar ATPγS binding affinities, with K_d values of ~0.1 μM, which were 10–20-fold tighter than the binding affinity for ADP (Fig. 2*B* and Table 2).

Multiple IBMPFD Mutations Do Not Have a Cumulative Effect on the Nucleotide-binding Properties at the D1 Site—So far, only single amino acid mutations in p97 have been reported in IBMPFD patients. We wondered if multiple IBMPFD mutations would have a cumulative effect on various properties of p97, particularly in nucleotide binding. To this end, we generated three mutants with double, triple, or even quadruple IBMPFD mutations in either the same domain or different

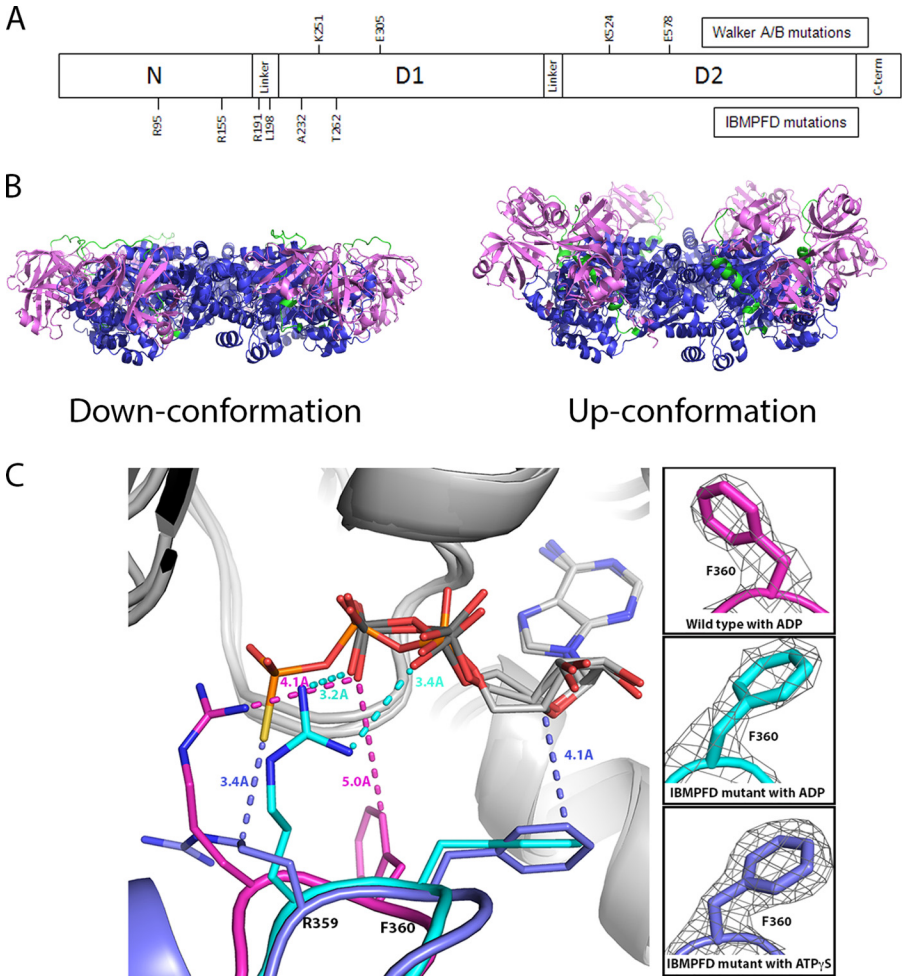

FIGURE 1. **Structure of the N-D1 fragment of p97 bearing IBMPFD mutations.** *A*, schematic drawing of p97 showing the domain arrangement and locations of the mutations used in the present study in the context of p97 primary sequence. One-letter amino acid codes are shown. The labels *N*, *D1*, and *D2* represent the N domain, the D1 domain, and the D2 domain, respectively. Also *labeled* are the locations of the Walker A/B mutations and the IBMPFD mutations used in the present study. *B*, *ribbon representation* of the structure of the hexameric p97 N-D1 fragment bearing the R155H mutation with bound ADP in the down-conformation and the A232E mutation with bound ATPγS in the up-conformation. N domains are shown in *magenta*, N-D1 linker in *green*, and the D1 domain in *blue*. *C*, alignment of the three p97 N-D1 structures (wild type with ADP bound (*magenta*, PDB code 1E32), R155H mutant with ADP bound (*cyan*), and R155H mutant with ATPγS bound (*blue*)), based on the superposition of bound nucleotides. The nucleotide-binding environment is shown, including the Walker A and B motifs (*gray*). The bound nucleotides (ADP and ATPγS) are shown as *stick models* with carbon in *light gray*, oxygen in *red*, nitrogen in *blue*, and sulfur in *yellow*. For the two ADP molecules, phosphorus atoms are shown in *dark gray*, and for the ATPγS, the phosphorus atoms are shown in *orange*. The SRH motifs of a neighboring subunit in the three aligned structures are shown in *magenta*, *blue*, and *cyan*, respectively, for wild type with ADP, mutant with ATPγS, and mutant with ADP. Side chains of residues Arg-359 and Phe-360 (*R359* and *F360*, respectively) are drawn as *stick models*. Distances between the nucleotide and Arg-359 or Phe-360 are *labeled*. *Insets*, side chains of Phe-360 in *stick models* from the three superimposed structures are overlaid with electron density meshes contoured at 1σ level from their respective $2F_o - F_c$ maps.

TABLE 1

ADP binding affinity (K_d) and stoichiometry (N) of various p97 mutants determined by ITC

The values are averaged over at least three independent titrations.

N-D1 p97 variant	K_d	Stoichiometry	Source/Ref.
	μM	N	
Wild type	0.88 ± 0.18	0.35 ± 0.06	Ref. 15
N domain			
R95G	2.27 ± 0.11	0.62 ± 0.08	Ref. 15
R155H	4.25 ± 0.54	0.72 ± 0.18	Ref. 15
N-D1 linker			
R191Q	2.56 ± 0.50	0.53 ± 0.06	This work
L198W	1.76 ± 0.17	0.65 ± 0.04	This work
D1 domain			
A232E	5.15 ± 1.38	0.71 ± 0.02	This work
T262A	3.59 ± 0.68	0.74 ± 0.04	This work

domains and determined their nucleotide-binding properties, including the binding affinities toward either ADP or ATPγS and the amount of prebound ADP (Table 3). To avoid potential misinterpretation, the mutations chosen were non-interacting and well separated in structure. The results from all three mutants showed they share similar characteristics with single mutations. They have less prebound ADP and reduced ADP binding affinity but similar binding affinity toward ATPγS as compared with the wild type protein. Therefore, no cumulative effect was observed in mutants carrying multiple IBMPFD mutations.

Comparison of Crystal Structures of Wild Type and Mutant p97 Reveals the Structural Basis of Altered Nucleotide Binding at the D1 Domain—IBMPFD mutations lead to a reduced amount of prebound ADP and a lower ADP binding affinity at the D1 sites compared with the wild type protein. To determine if structural changes in the vicinity of the D1 nucleotide-binding sites contribute to these differences in nucleotide-binding properties, we compared the high resolution structure of wild type p97 with those of IBMPFD mutants with bound ADP or ATPγS. Crystal structures of wild type p97, both the N-D1 frag-

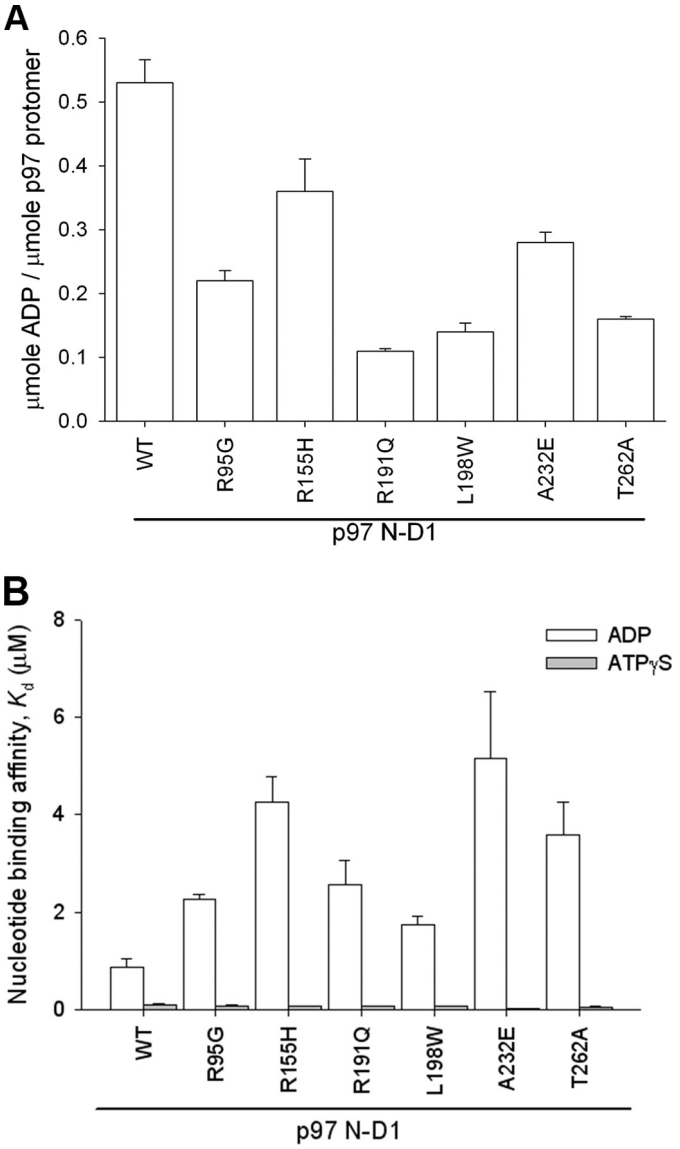

FIGURE 2. **Reduction in prebound ADP and in ADP-binding affinity for IBMPFD mutants.** *A*, amount of prebound ADP for p97 N-D1 fragments. Amounts of prebound ADP at the D1 domain of wild type and IBMPFD mutants were determined by heat denaturation followed by MonoQ ion-exchange chromatography on FPLC. *B*, nucleotide-binding affinity (K_d) at the D1 domain determined by ITC for wild type and various mutants. The ATPγS binding affinity (K_d) measured by ITC is provided for p97 N-D1 variants treated with apyrase. *Error bars*, S.D.

ment (PDB code 1E32) (16) and full length (PDB codes 3CF1 and 1R7R) (11, 12), were determined with only ADP bound to the D1 domain. We reported crystal structures of N-D1 fragments of three p97 mutants (R95G, R155H, and R86A) with bound ATPγS and for R155H with ADP bound (15). It is important to note that all of these mutations are in the N domain. In this work, we present for the first time the crystal structure of the N-D1 fragment bearing the mutation A232E in the D1 domain in the presence of ATPγS determined to 2.6 Å resolution (Table 4). The structure was solved by the molecular replacement method and refined to R_{free} and R_{work} values of 27.5 and 28.9%, respectively. We also obtained diffraction data sets at much higher resolution, 2.95 and 1.98 Å, respectively, for the R155H mutant with bound ADP and ATPγS (Table 4).

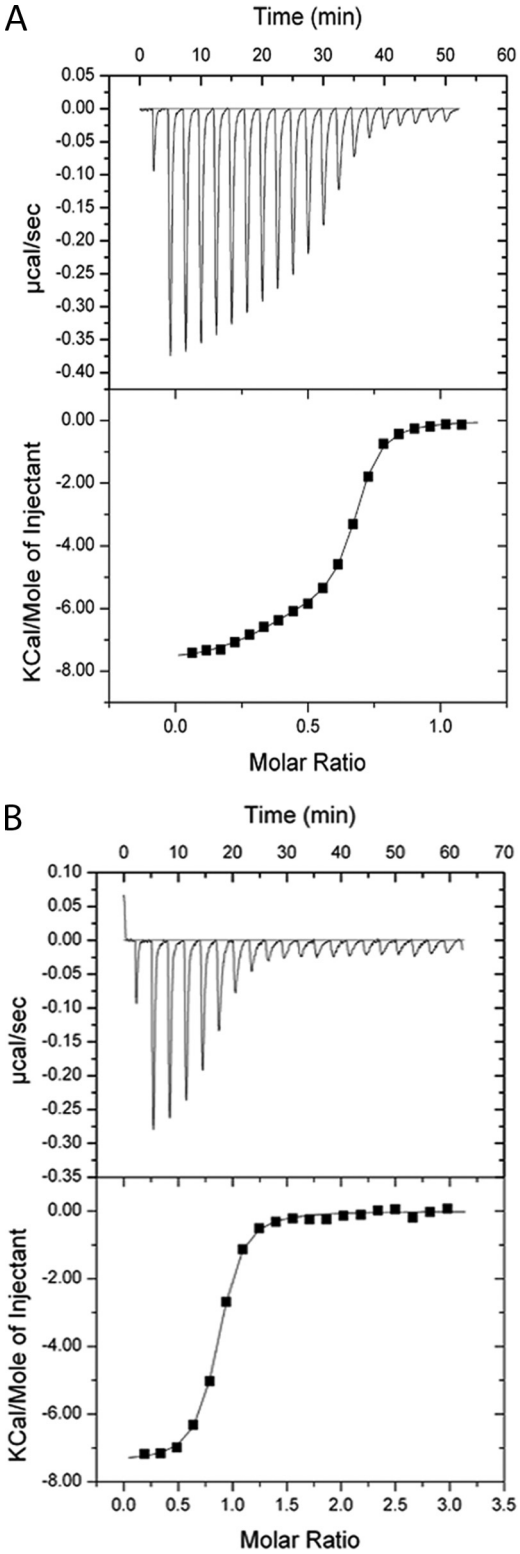

FIGURE 3. **ATPγS binding property to D1 domains of p97 variants.** *A*, exothermal profile of ATPγS titration measured by ITC for the untreated N-D1 truncate bearing the L198W mutation. 19 injections of 10 μl each of 150 μM ATPγS solution were mixed with 1.4236 ml of 20 μM protein solution (*top*). The data were fitted (*bottom panel*) using the two-type of site model implemented in Origin® version 7 with both affinity constant K_a and binding stoichiometry *N* as variables. *B*, ITC profile of apyrase-treated L198W p97 N-D1 mutant titrated with ATPγS. 19 injections of 7 μl of 150 μM ATPγS solution were mixed with 1.4236 ml of 5 μM protein solution (*top*). The data were fitted (*bottom*) using the one-type of site model implemented in Origin® version 7.

Structures corresponding to these data sets were further refined (Table 4) and used for subsequent analysis. Notably, the two ATPγS-bound structures were determined in two different crystal forms (Table 4) with very different crystal packing environments. The R155H mutant forms crystals that have the symmetry of the *R*3 space group and diffract x-rays to high resolution but are merohedrally twined. The structure of the ADP-bound form was also derived from the crystal form different from wild type p97 previously reported (11, 12, 16). Thus, it is unlikely that the nucleotide-dependent N domain conformational change (see below) observed in this work is a result of crystal packing.

As observed previously for the IBMPFD mutants R95G and R155H, the N domains for the A232E mutant also uniformly take the up-conformation in the ATPγS bound form (Fig. 1*B*). Thus, the observation of a nucleotide-dependent N domain conformational switch can extend to the mutation that occurs at the D1 domain as well, which is consistent with experimental observations that all IBMPFD mutants behave similarly in their nucleotide-binding properties.

Although large, uniform conformational changes were observed for N domains and N-D1 linkers in the structure superposition between the two conformations of the same mutant (15), no significant changes were observed in the immediate vicinity of the nucleotide-binding pocket of the D1

TABLE 2

Binding affinity toward ATPγS for apyrase-treated p97 N-D1 fragments as determined by ITC

The values are averaged over at least three independent titrations.

p97 N-D1	K_d	Stoichiometry
	μM	N
Wild type	0.11 ± 0.01	1.20 ± 0.02
R95G	0.09 ± 0.01	1.10 ± 0.05
R155H	0.07 ± 0.01	1.20 ± 0.05
R191Q	0.08 ± 0.01	0.91 ± 0.07
L198W	0.07 ± 0.01	0.94 ± 0.10
A232E	0.02 ± 0.001	0.99 ± 0.01
T262A	0.06 ± 0.02	0.99 ± 0.04

TABLE 3

Nucleotide-binding properties of p97 N-D1 proteins having multiple IBMPFD mutations

The values are averaged over at least three independent experiments.

p97 N-D1	ADP		ATPγS[a]		Amount of prebound ADP
	K_d	Stoichiometry	K_d	Stoichiometry	
	μM	N	μM	N	μmol ADP/μmol p97 protomer
Wild type	0.88 ± 0.18	0.35 ± 0.06	0.11 ± 0.01	1.20 ± 0.02	0.53 ± 0.036
R95G/R155H	4.37 ± 0.96	0.64 ± 0.05	0.08 ± 0.01	1.36 ± 0.02	0.16 ± 0.017
R95G/R155H/A232E	2.51 ± 0.25	0.73 ± 0.05	0.06 ± 0.01	1.38 ± 0.04	0.07 ± 0.004
R95G/R155H/A232E/R191Q	2.96 ± 0.12	0.43 ± 0.02	0.10 ± 0.02	1.34 ± 0.01	0.13 ± 0.018

[a] Samples were pretreated with apyrase to remove prebound ADP at D1 sites before the ITC experiments.

TABLE 4

Statistics on the quality of diffraction data sets and refined atomic models

	R155H	R155H	A232E
Bound nucleotide	ATPγS	ADP	ATPγS
Data collection			
Space group	*R*3	$P2_12_12_1$	*P*1
Cell units (Å)	a = 134.2, b = 134.2, c = 182.9	a = 146.5, b = 170.4, c = 256.6	a = 91.1, b = 104.6, c = 109.5
Cell units (degrees)	α = 0.0, β = 90.0, γ = 120.0	α = 90.0, β = 90.0, γ = 90.0	α = 98.1, β = 90.5, γ = 92.7
Resolution (last shell) (Å)	50-1.98 (2.05-1.98)	50-2.95 (3.06-2.95)	100-2.60 (2.69-2.60)
R_{merge}[a] (last shell) (%)	5.1 (52.4)[b]	9.3 (47.0)	8.9 (53.1)
Completeness (last shell) (%)	93.4 (69.5)	88.1 (51.3)	85.7 (70.4)
Total observations	234,496	540,585	266,983
Unique reflections	79,692	118,808	101,600
$I/\sigma(I)$ (last shell)	20.2 (1.1)	8.5 (1.3)	8.4 (1.0)
Refinement statistics			
Resolution (Å)	98-1.98	20-2.96	46.3-2.62
R_{free} (last shell) (%)	19.4 (26.4)[c]	29.1 (52.5)	28.9 (50.1)
R_{work} (last shell) (%)	20.5 (26.2)	26.8 (52.1)	27.5 (52.2)
Root mean square bond length (Å)	0.007	0.008	0.005
Root mean square bond angle (degrees)	1.09	1.26	1.12
Root mean square coordinate error (R_{free}) (Å)	0.028	0.534	0.390
Root mean square no. of non-hydrogen atoms	7,392	41,760	21,556
No. of residues	900	5,271	2,706
No. of NCS-related subunits	2	12	6
No. of solvent molecules	279	168	166
No. of ATPγS/ADP	2	12	6
No. of Mg^{2+} ions	2	0	6
PDB code	4KO8	4KOD	4KLN
Ramachandran analysis[d]			
Most favored (%)	90.0	89.8	90.1
Allowed (%)	10.0	9.9	9.9
Generously allowed (%)	0	0.3	0
Disallowed (%)	0	0	0

[a] R_{merge} is defined as $\Sigma|I_{h,i} - \langle I_h \rangle| / \Sigma I_{h,i}$, where $I_{h,i}$ is the intensity for the *i*th observation of a reflection with Miller index *h*, and $\langle I_h \rangle$ is the mean intensity for all measured I_h values and Friedel pairs.

[b] Values in parentheses are for the highest resolution shells.

[c] The crystal is a merohedral twin with a twin factor of 0.6 relating *h*,*k*,*l* to *h*,−*h*−*k*,−*l*. A consequence of a sharpened intensity distribution in cases of twinned crystals, the *R*-factors are lower than in cases of non-twinned crystals.

[d] Ramachandran plot analysis was performed by the program PROCHECK (17).

domain. However, structural alignment between wild type (ADP-bound) (PDB code 1E32) (16) and mutant (either ADP- or ATPγS-bound) revealed changes that might account for the altered nucleotide binding in the mutants. When the wild type structure was superimposed on the mutant structure based on the alignment of bound nucleotides, major differences in the vicinity of the bound nucleotides were the side chain conformations of residues Arg-359 and Phe-360, which jut into the nucleotide-binding site of the adjacent subunit (Fig. 1*C*). Both residues contribute to a conserved motif, referred to as the second region of homology (SRH), that distinguishes AAA proteins from other ATPases (40). The phenyl side chains of Phe-360 in all structures are well ordered, as shown Fig. 1*C* (*insets*). In the wild type, the phenyl side chain of Phe-360 points away from the bound ADP and at its closest distance is 5.0 Å from an oxygen atom of the β-phosphate, whereas in the mutants with either bound ADP or ATPγS, the phenyl side chain is rotated nearly 120° around the χ1 dihedral axis to face the ribose moiety of the bound nucleotide at an average distance of 3.8 Å. In the mutant with bound ADP, the guanidinium side chain of the Arg finger residue Arg-359 is refined to a position interacting with both α-phosphate (3.2 Å) and β-phosphate (3.3 Å) of the bound nucleotide, whereas in both the wild type with bound ADP and the mutant with bound ATPγS, the side chain of Arg-359 only makes contact with the terminal phosphate of the bound nucleotide (4.1 Å to β-phosphate of ADP and 3.4 Å to γ-phosphate of ATPγS). Thus, in mutants, it appears that the phenyl side chain of Phe-360 is unable to undergo the conformational change required to respond to the changes in bound nucleotide at the D1 domain, and that of Arg-359 behaves aberrantly in the presence of ADP.

IBMPFD Mutations Enhance the ATPase Activity in the D2 Domain—Conflicting observations on the effect of IBMPFD mutations on the ATPase activity of p97 have been reported. Although some reports have shown that pathogenic mutants have ATPase activities similar to that of the wild type (6, 21), others have demonstrated significantly enhanced ATPase activity (19, 20, 22). No mechanistic interpretation has been offered in the latter reports as to why the ATPase activity is elevated. To resolve this controversy and to investigate how IBMPFD mutations may interfere with ATP hydrolysis of p97, we took a different approach by measuring ATPase activities for both N-D1 truncates and full-length proteins. Because mutations are found only in the N-D1 domains of p97 and remote from the D2 domain, this approach would segregate the ATPase activity contributed by the D1 ring from that of D2 and thus simplify the interpretation of how mutations alter ATPase activities.

First, we measured ATPase activities of the N-D1 fragments of the wild type and the six selected IBMPFD mutants. In the presence of just one ATPase domain, all N-D1 IBMPFD mutants showed only a slight increase in ATPase activity ranging from 1.1-fold (L198W) to 1.8-fold (T262A), when compared with the wild type protein (Fig. 4*A*). Clearly, the effect of mutations on D1 domain ATPase activity is moderate but real because no product inhibition was detected (data not shown). Next, we measured ATPase activities of full-length p97 for both wild type and the set of mutants. In agreement with most reports, all IBMPFD mutants exhibited higher, albeit to different extents, ATPase activities than the wild type p97, with 1.7-fold (R191Q) to 2.6-fold (R155H) higher activity, depending on the site of mutation (Fig. 4*B*), demonstrating that the enhancement in ATPase activity in the IBMPFD mutants is mainly from the D2 domain. Additionally and perhaps more importantly, the magnification of ATPase activity by the full-length p97 supports the existence of a communication pathway that connects the site of mutation to the distal D2 domain.

The Intrasubunit Communication between D1 and D2 Domains Is Preserved in IBMPFD Mutants—To further confirm the existence of a communication pathway between the two cognate ATPase domains within a subunit and to explore the effect of mutations on this pathway, point mutations in Walker A or Walker B motifs were introduced to each domain of both the wild type and two of the IBMPFD mutants. The Walker A mutations (K251T and K524T) are known to reduce the binding of nucleotide to their respective ATPase domains, whereas the Walker B mutations (E305Q and E578Q) do not affect nucleotide binding but rather effectively inhibit ATP hydrolysis (41–43). The effectiveness of either Walker A (K251T) or Walker B (E305Q) mutation in abolishing ATPase activity was demonstrated first in the wild type N-D1 fragment (containing only the D1 ATPase domain), in which no ATPase activity was detected for either Walker A or B mutants (Fig. 4*C*). When the E305Q Walker B mutation was introduced into full-length p97, the ATPase activity was the same as that of wild type p97. Because only the D2 site is functional in this mutant, these data imply that binding of nucleotide to the D1 site enhances activity in D2. By contrast, when the K251T Walker A mutation was introduced into the D1 site in full-length p97, the ATPase activity was only 15% of the wild type activity (Fig. 4*C*), consistent with the proposal that nucleotide binding to the D1 site promotes the activity at D2. We also noticed that the presence of the D2 domain restrains the ATP hydrolysis activity of the D1 domain (Fig. 4*C*), because the wild type N-D1 displays higher ATPase activity than the full-length protein bearing the D2 Walker A mutation K524T. Similar observations were made previously (14, 43) and suggest that binding of nucleotide at one ATPase domain is essential for the activity of the other. In other words, the two ATPase domains in p97 regulate each other's activities during the ATP hydrolysis cycle. Consistent with this model, the Walker B mutant (E578Q) of the D2 domain, which retains the ability to bind but not to hydrolyze ATP, stimulated ATPase activity in D1 (Fig. 4*C*).

To investigate the potential effect of the IBMPFD mutations on the above communication pathway between the two cognate ATPase domains and to seek a mechanistic explanation for the observed enhancement in ATPase activity for IBMPFD mutants, Walker A/B mutations were introduced into two IBMPFD mutants (R95G and R191Q), and their ATPase activities were determined. The effect of Walker A/B mutations on the ATPase activity of IBMPFD mutants appears to be very similar to that of the wild type p97 bearing the same Walker A/B mutations (Fig. 4*D*). A Walker A mutation in either domain (K251T or K524T) greatly reduced the ATPase activities of the IBMPFD mutants. The Walker B mutation (E305Q) in the D1 domain does not have much effect on the ATPase activity, whereas the E578Q mutation in the D2 domain significantly reduces the activity of the IBMPFD mutants (Fig. 2*D*).

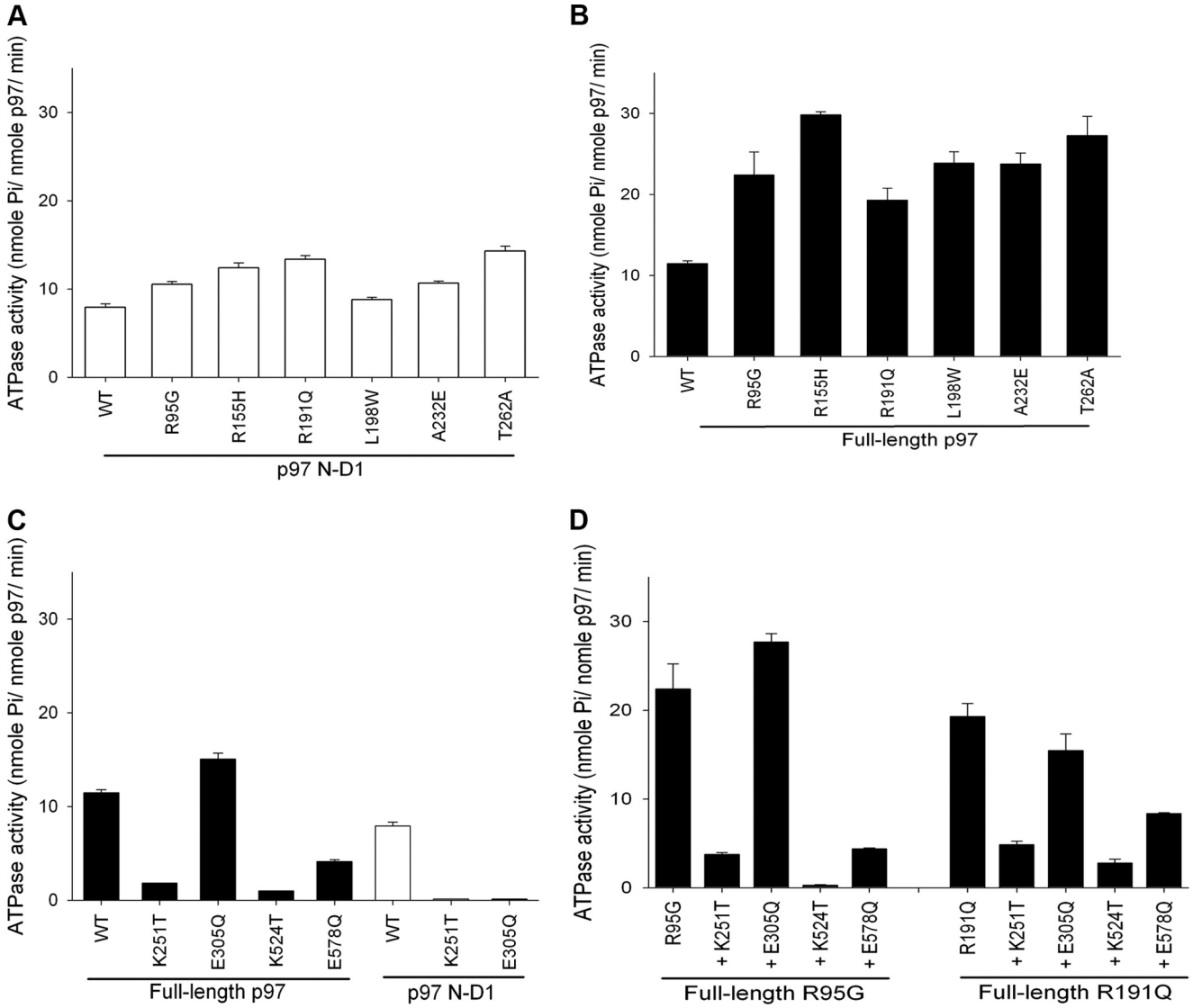

FIGURE 4. **ATPase activities of p97 wild type and variants.** In *all panels*, *white bars* represent activities for p97 N-D1 truncates, and *black bars* represent full-length p97. *A*, N-D1 fragments of p97 bearing IBMPFD mutations. *B*, full-length p97 bearing IBMPFD mutations. *C*, different constructs, either N-D1 or full-length, of p97 bearing Walker A (K251T or K524T) or Walker B (E305Q or E578Q) mutations. *D*, IBMPFD mutants R95G and R191Q bearing Walker A or Walker B mutations. *Error bars*, S.D.

These results suggest that the IBMPFD mutations do not interrupt the communication between the cognate D1 and D2 domains because the signature enhancement in ATPase activity by IBMPFD mutations is retained even when the D1 domain is incapable of hydrolyzing ATP (E305Q), which again suggests that enhancement of the ATPase activity in the IBMPFD mutants is mainly due to the distal D2 domain.

DISCUSSION

The p97 molecular machine consists of 18 discrete domains (six sets of three domains); these domains must communicate with each other in order to work properly. Conceivably, at least two modes of communication may exist within the p97 machine: intrasubunit and intersubunit. By comparing the structural and functional differences between the wild type and IBMPFD mutant p97, it became obvious that this network of communication pathways is intricate and capable of regulating the function of different domains in p97.

Intra- and Intersubunit Regulation of p97—Previous studies hinted at the presence of communication among cognate domains in p97. For example, binding of adaptor protein p47 reduces the ATPase activity of p97 (44). Also, the presence of the D2 domain inhibits nucleotide exchange in the D1 domain (14), and binding of nucleotide in D1 is required for ATP binding at the D2 domain (43). Similar observations have been made in Cdc48.1, a p97 homolog in *Caenorhabditis elegans* (23). In this work, we confirmed that in wild type p97 ATP hydrolysis of the D2 domain requires binding of nucleotide at the D1 domain (Fig. 4*C*), and the presence of the D2 domain inhibits the ATPase activity of the D1 domain (Fig. 4*C*). Thus, these results can be interpreted as evidence for the presence of intrasubunit communication among domains of a p97 subunit.

Studies also indicate that the subunits within the p97 hexamer regulate each other. Such communication can take place at the nucleotide-binding site, mediated via the secondary region of homology (SRH) motifs. The motif is conserved in a

subclass of the AAA family proteins and features conserved Arg finger residues that project into the nucleotide-binding site of neighboring subunits (40, 42). Thus the Arg fingers in the SRH motif are considered part of the intersubunit communication pathway. In p97, the two AAA domains each feature an SRH motif with Arg finger residues Arg-359 and Arg-362 for the D1 domain and Arg-635 and Arg-638 for the D2 domain (45). The strong association of the D1 domains to form a hexameric ring is also indicative of the role of D1 Arg finger residues in the intersubunit communication.

In addition, it is known that in wild type p97, the nucleotide states of D1 domains are under tight control, as shown by the presence of prebound ADP found in 30–50% of the D1 domains (11, 38). Furthermore, ATPγS can only bind to empty D1 sites and cannot displace the prebound ADP (15), resulting in heterogeneous nucleotide states at the D1 domain within a hexamer. Since the movement of the N domain is controlled by the nucleotide state of the D1 domain (15), the non-uniformity of the nucleotide state of D1 domains extends to the conformations of their cognate N domains. This heterogeneity in N domain conformation seems to be a crucial property for the function of wild type p97, which is disrupted, because we observed instead a uniform N domain conformation in pathogenic p97.

IBMPFD Mutants Have a Defect in the Intersubunit Communication—Systematic studies on full-length p97 bearing various IBMPFD mutations have consistently shown elevated ATPase activity although to different extents for different mutations (Fig. 4*B*). Because all mutation sites are remote from the D1 and D2 nucleotide-binding pockets, it was tempting to speculate that the mutations may have altered the intrasubunit communication pathway. However, by studying the Walker motif mutations, we concluded that the intrasubunit communication seems well preserved in the IBMPFD mutants, because it displays the same pattern of ATPase activities as the wild type (Figs. 4, *C* and *D*).

On the other hand, by choosing a set of IBMPFD mutations that are located at different domains of p97 and studying their nucleotide binding and hydrolysis properties, we became convinced that the IBMPFD mutations most likely lead to defects in the intersubunit communication. First, all pathogenic p97 mutants have a lower amount of prebound ADP at the D1 domain when compared with the wild type (Fig. 2*A*). Second, the sites with ADP prebound become accessible to ATPγS in pathogenic p97 but not in wild type. These suggest a tight regulation of the D1 domain nucleotide state of wild type p97 and coordination among neighboring subunits, restricting displacement of prebound ADP by ATPγS. With IBMPFD mutations, such a regulation is disrupted. Instead of working coordinately, the D1 domains of pathogenic p97 work more or less independently, as evidenced by the crystal structures of mutants with uniformly bound ATPγS at the D1 domain (Fig. 1*B*) (15). The uniform nucleotide state as a consequence of defective regulation in IBMPFD mutants is thus naturally followed by uniform N domain conformation, as so compellingly shown by these structures (Fig. 1*B*), because the conformation of each N domain is dependent on the nucleotide state of its cognitive D1 domain.

```
                                  ↓
p97-D1      347 TNRPNSIDPALRRFGRFDREVDIGIPD 373
cdc48-D1    357 TNRPNSIDPALRRFGRFDREVDIGIPD 383
p97-        623 TNRPDIIDPAILRPGRLDQLIYIPLPD 649
cdc48-D2    633 TNRPDQIDPAILRPGRLDQLIYVPLPD 659
Paraplegin  455 TNRADILDGALMRPGRLDRHVFIDLPT 481
NSF         373 TNRPDLIDEALLRPGRLEVKMEIGLPD 399
VAT         333 TNRIDAIDPALRRPGRFDREIEIGVPD 359
PAN         316 TNRPDILDPAILRPGRFDRIIEVPAPD 342
FtsH        301 TNRPDILDPALLRPGRFDRQIAIDAPD 327
```

FIGURE 5. **Sequence alignment for various AAA proteins in the neighborhood of the SRH region.** The *arrow* indicates the position of residue Phe-360.

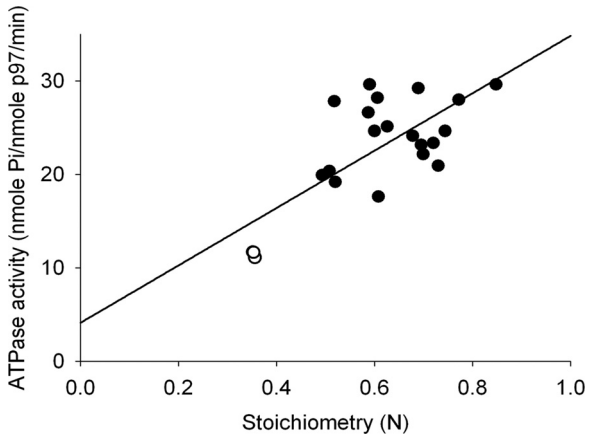

FIGURE 6. **Correlation between specific ATPase activities of full-length p97 and the measured available sites for ADP titration at the D1 domain for wild type and mutants.** The full-length ATPase activities were taken from data shown in Fig. 4*B*, and the values for binding stoichiometry were obtained from ADP titration to N-D1 p97 fragments using ITC (data from Table 1). Data points from each individual experiment were plotted and fitted using a linear regression model by least squares. *Closed circles*, IBMPFD mutants; *open circles*, wild type p97.

Structural Basis for the Reduced ADP Binding Affinity in IBMPFD Mutants—Previously, we showed that only in IBMPFD mutants can all six N domains adopt the up-conformation that is dependent on the binding of ATPγS to the D1 domain; this was demonstrated by the crystal structures of IBMPFD mutants R155H and R95G, both in the N domain (15, 39). In this work, we present the crystal structure of mutant A232E, in which the mutation is located in the D1 domain, in the presence of ATPγS. The new structure reinforced our prior observations of nucleotide-dependent N domain conformation and a likely defect in intersubunit communication in IBMPFD mutants. Available data reveal that the primary change in IBMPFD mutants is the reduction of ADP binding to the D1 domain, which results in various secondary effects, such as uniform N domain conformation and enhanced ATPase activities. But what is the structural basis for the reduced ADP binding affinity in IBMPFD mutants?

Structure comparison between the wild type p97 with bound ADP in the D1 domain and mutants in either ADP- or ATPγS-bound forms revealed a different side chain conformation for Phe-360 that is part of the SRH motif (Fig. 1*C*). Because the crystal structure of wild type p97 with ATPγS bound at the D1 domain is not available, it is not certain whether the side chain conformation of Phe-360 in wild type p97 would be the same as that for mutant bound with ATPγS. Nevertheless, the very sim-

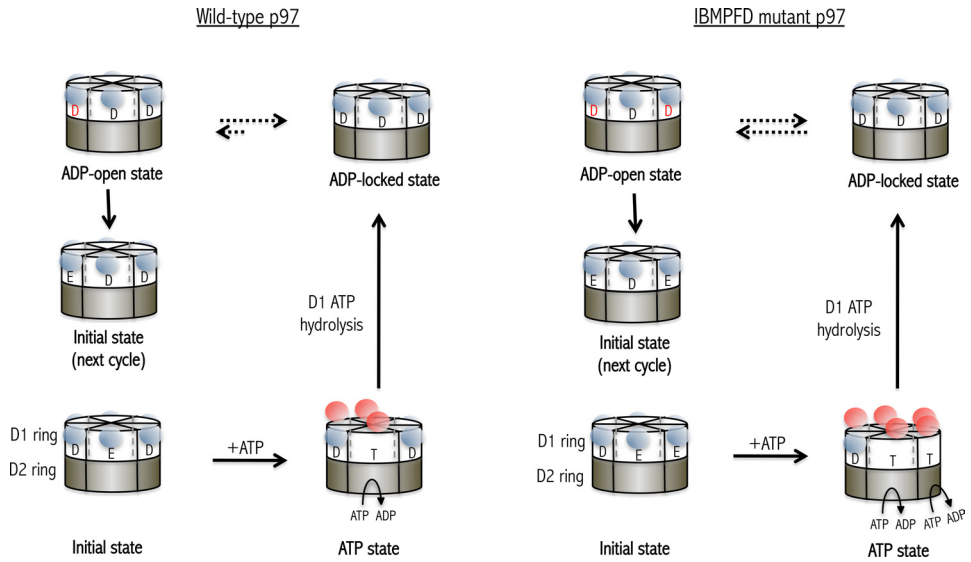

FIGURE 7. **Schematic presentation of the model proposed for the control of N domain movement and ATPase activity in the D2 domain of p97.** N domains are shown as *blue* and *red spheres* in the down- and up-conformation, respectively. D1 and D2 rings are represented by *light* and *dark gray cylinders*, respectively, and *labeled*. We propose that the intersubunit communication is conducted in the D1 ring, and the intrasubunit communication is carried out within each p97 subunit. For each subunit, there are four nucleotide-binding states in the D1 domain, as indicated. In both the ADP-open and ADP-locked states, the D1 sites are occupied by ADP, and the N domain is in the down-conformation. However, the bound ADP can only be displaced by ATP in the ADP-open state (*D* in *red*). In the wild type p97, there is a tight regulation, perhaps by neighboring subunits, between the ADP-open and ADP-locked states with a significant portion of D1 domains in the ADP-locked state. The initial state is a state where no nucleotide is bound to D1 domains of some subunits within the ring, as indicated by *E*. In the ATP state, ATP binding to the D1 domain, indicated by *T*, triggers the N domains to adopt the up-conformation in corresponding subunits. In IBMPFD mutants, the control over the D1 domain favors the ADP-open state, allowing binding of ATP to more D1 sites and leading to more D2 domains engaging in ATP hydrolysis.

ilar affinities for ATPγS binding to D1 domains in all variants of p97 tested (Table 2) make it reasonable to assume that the phenyl ring of Phe-360 undergoes conformational changes in accordance with the type of nucleotide bound to the D1 domain of a neighboring subunit in wild type p97. Thus, the observation that in IBMPFD mutants, Phe-360 has its side chain fixed in a single conformation, losing its ability to discriminate between bound ADP and ATP, could provide a possible explanation for the reduction of ADP binding affinity in mutants. In this fixed conformation, the phenyl side chain of Phe-360 is closer to bound ADP (average of 3.8 Å) than in the other conformation (5.0 Å). Therefore, it is conceivable that the electron-rich phenyl ring exerts a repelling force to the negatively charged ADP bound at the site, leading to reduction in binding affinity. Sequence alignment of AAA members (Fig. 5) shows that Phe-360 is conserved only in mammalian p97 and in the yeast Cdc48 D1 domain, suggesting a distinct role for this residue pertaining to the function of the D1 domain in mammalian p97 and yeast Cdc48. In light of this, it is tempting to speculate that Phe-360 in p97 has evolved to play a role in sensing the occupants in the nucleotide-binding site of a neighboring subunit. This speculation is consistent with the designation of an intersubunit signaling motif (28, 29), which provides a residue (Asp-333) to form a salt bridge with the Arg finger residue Arg-359 next to Phe-360.

Enhanced ATPase Activity in IBMPFD Mutants Is Correlated with the Availability of Nucleotide-binding Sites of the D1 Domain—In this work, we showed that IBMPFD mutations invariably lead to elevated ATPase activities, mostly from the D2 domain (Fig. 4*B*), corroborating previous observations (19, 20, 22). We noticed that the enhancement in ATPase activity is not uniform across all IBMPFD mutants. Because the D2 domain ATPase activity is dependent on the binding of nucleotide to the D1 domain, we surmise that the increased number of available D1 sites in mutants may be the cause for the elevated ATPase activity in D2. Indeed, a linear correlation was observed between the number of ADP titratable sites in the D1 domain and the measured ATPase activities (Fig. 6), with a computed Pearson correlation coefficient of 0.73. Because a strong correlation does not necessarily reflect true causality, this conclusion should be taken with caution. Nevertheless, if this were true, it would also predict that ATP must bind to the D1 site in order to stimulate the ATPase activity in the D2 ring (Fig. 7). Thus, the enhanced ATPase activity observed in the IBMPFD mutants could be the consequence of more D2 domains taking part in ATP hydrolysis (Fig. 7). Although a direct experimental demonstration is yet to be obtained, circumstantial evidence does exist. For instance, experimentally locking N domains of p97 to the down-conformation was shown to inhibit its overall ATPase activity (20), probably by blocking the access of ATP to the D1 domain.

Acknowledgments—We thank Drs. Michael Maurizi (NCI, National Institutes of Health) and Yihong Ye (NIDDK, National Institutes of Health) for careful reading of the manuscript. We appreciate the help from staff of the SER-CAT beam line of the Advance Photon Source, Argonne National Laboratory, in assisting with x-ray diffraction data collection, and we also thank George Leiman for editorial assistance.

REFERENCES

1. Watts, G. D., Wymer, J., Kovach, M. J., Mehta, S. G., Mumm, S., Darvish, D., Pestronk, A., Whyte, M. P., and Kimonis, V. E. (2004) Inclusion body

myopathy associated with Paget disease of bone and frontotemporal dementia is caused by mutant valosin-containing protein. *Nat. Genet.* **36,** 377–381
2. Tang, W. K., and Xia, D. (2012) IBMPFD and p97, the structural and molecular basis for functional disruption. in *Neuromuscular Disorders* (Zaher, A., ed) pp. 155–174, InTech, Rijeka, Croatia
3. Nalbandian, A., Donkervoort, S., Dec, E., Badadani, M., Katheria, V., Rana, P., Nguyen, C., Mukherjee, J., Caiozzo, V., Martin, B., Watts, G. D., Vesa, J., Smith, C., and Kimonis, V. E. (2011) The multiple faces of valosin-containing protein-associated diseases. Inclusion body myopathy with Paget's disease of bone, frontotemporal dementia, and amyotrophic lateral sclerosis. *J. Mol. Neurosci.* **45,** 522–531
4. Gu, J. M., Ke, Y. H., Yue, H., Liu, Y. J., Zhang, Z., Zhang, H., Hu, W. W., Wang, C., He, J. W., Hu, Y. Q., Li, M., Fu, W. Z., and Zhang, Z. L. (2013) A novel VCP mutation as the cause of atypical IBMPFD in a Chinese family. *Bone* **52,** 9–16
5. Kimonis, V. E., Mehta, S. G., Fulchiero, E. C., Thomasova, D., Pasquali, M., Boycott, K., Neilan, E. G., Kartashov, A., Forman, M. S., Tucker, S., Kimonis, K., Mumm, S., Whyte, M. P., Smith, C. D., and Watts, G. D. (2008) Clinical studies in familial VCP myopathy associated with Paget disease of bone and frontotemporal dementia. *Am. J. Med. Genet. A* **146A,** 745–757
6. Weihl, C. C., Dalal, S., Pestronk, A., and Hanson, P. I. (2006) Inclusion body myopathy-associated mutations in p97/VCP impair endoplasmic reticulum-associated degradation. *Hum. Mol. Genet.* **15,** 189–199
7. Ju, J. S., Fuentealba, R. A., Miller, S. E., Jackson, E., Piwnica-Worms, D., Baloh, R. H., and Weihl, C. C. (2009) Valosin-containing protein (VCP) is required for autophagy and is disrupted in VCP disease. *J. Cell Biol.* **187,** 875–888
8. Vesa, J., Su, H., Watts, G. D., Krause, S., Walter, M. C., Martin, B., Smith, C., Wallace, D. C., and Kimonis, V. E. (2009) Valosin containing protein associated inclusion body myopathy. Abnormal vacuolization, autophagy and cell fusion in myoblasts. *Neuromuscul. Disord.* **19,** 766–772
9. Tresse, E., Salomons, F. A., Vesa, J., Bott, L. C., Kimonis, V., Yao, T. P., Dantuma, N. P., and Taylor, J. P. (2010) VCP/p97 is essential for maturation of ubiquitin-containing autophagosomes and this function is impaired by mutations that cause IBMPFD. *Autophagy* **6,** 217–227
10. Ritz, D., Vuk, M., Kirchner, P., Bug, M., Schütz, S., Hayer, A., Bremer, S., Lusk, C., Baloh, R. H., Lee, H., Glatter, T., Gstaiger, M., Aebersold, R., Weihl, C. C., and Meyer, H. (2011) Endolysosomal sorting of ubiquitylated caveolin-1 is regulated by VCP and UBXD1 and impaired by VCP disease mutations. *Nat. Cell Biol.* **13,** 1116–1123
11. DeLaBarre, B., and Brunger, A. T. (2003) Complete structure of p97/valosin-containing protein reveals communication between nucleotide domains. *Nat. Struct. Biol.* **10,** 856–863
12. Huyton, T., Pye, V. E., Briggs, L. C., Flynn, T. C., Beuron, F., Kondo, H., Ma, J., Zhang, X., and Freemont, P. S. (2003) The crystal structure of murine p97/VCP at 3.6 Å. *J. Struct. Biol.* **144,** 337–348
13. Rouiller, I., DeLaBarre, B., May, A. P., Weis, W. I., Brunger, A. T., Milligan, R. A., and Wilson-Kubalek, E. M. (2002) Conformational changes of the multifunction p97 AAA ATPase during its ATPase cycle. *Nat. Struct. Biol.* **9,** 950–957
14. Davies, J. M., Tsuruta, H., May, A. P., and Weis, W. I. (2005) Conformational changes of p97 during nucleotide hydrolysis determined by small-angle x-ray scattering. *Structure* **13,** 183–195
15. Tang, W. K., Li, D., Li, C. C., Esser, L., Dai, R., Guo, L., and Xia, D. (2010) A novel ATP-dependent conformation in p97 N-D1 fragment revealed by crystal structures of disease-related mutants. *EMBO J.* **29,** 2217–2229
16. Zhang, X., Shaw, A., Bates, P. A., Newman, R. H., Gowen, B., Orlova, E., Gorman, M. A., Kondo, H., Dokurno, P., Lally, J., Leonard, G., Meyer, H., van Heel, M., and Freemont, P. S. (2000) Structure of the AAA ATPase p97. *Mol. Cell* **6,** 1473–1484
17. Laskowski, R. A., MacArthur, M. W., Moss, D. S., and Thornton, J. M. (1993) PROCHECK. A program to check the stereochemical quality of protein structures. *J. Appl. Cryst.* **26,** 283–291
18. DeLaBarre, B., and Brunger, A. T. (2005) Nucleotide dependent motion and mechanism of action of p97/VCP. *J. Mol. Biol.* **347,** 437–452
19. Halawani, D., LeBlanc, A. C., Rouiller, I., Michnick, S. W., Servant, M. J., and Latterich, M. (2009) Hereditary inclusion body myopathy-linked p97/VCP mutations in the NH2 domain and the D1 ring modulate p97/VCP ATPase activity and D2 ring conformation. *Mol. Cell Biol.* **29,** 4484–4494
20. Niwa, H., Ewens, C. A., Tsang, C., Yeung, H. O., Zhang, X., and Freemont, P. S. (2012) The role of the N-domain in the ATPase activity of the mammalian AAA ATPase p97/VCP. *J. Biol. Chem.* **287,** 8561–8570
21. Fernández-Sáiz, V., and Buchberger, A. (2010) Imbalances in p97 co-factor interactions in human proteinopathy. *EMBO Rep.* **11,** 479–485
22. Manno, A., Noguchi, M., Fukushi, J., Motohashi, Y., and Kakizuka, A. (2010) Enhanced ATPase activities as a primary defect of mutant valosin-containing proteins that cause inclusion body myopathy associated with Paget disease of bone and frontotemporal dementia. *Genes Cells* **15,** 911–922
23. Nishikori, S., Esaki, M., Yamanaka, K., Sugimoto, S., and Ogura, T. (2011) Positive cooperativity of the p97 AAA ATPase is critical for essential functions. *J. Biol. Chem.* **286,** 15815–15820
24. Martin, A., Baker, T. A., and Sauer, R. T. (2005) Rebuilt AAA+ motors reveal operating principles for ATP-fuelled machines. *Nature* **437,** 1115–1120
25. Enemark, E. J., and Joshua-Tor, L. (2006) Mechanism of DNA translocation in a replicative hexameric helicase. *Nature* **442,** 270–275
26. Moreau, M. J., McGeoch, A. T., Lowe, A. R., Itzhaki, L. S., and Bell, S. D. (2007) ATPase site architecture and helicase mechanism of an archaeal MCM. *Mol. Cell* **28,** 304–314
27. Werbeck, N. D., Schlee, S., and Reinstein, J. (2008) Coupling and dynamics of subunits in the hexameric AAA+ chaperone ClpB. *J. Mol. Biol.* **378,** 178–190
28. Augustin, S., Gerdes, F., Lee, S., Tsai, F. T., Langer, T., and Tatsuta, T. (2009) An intersubunit signaling network coordinates ATP hydrolysis by m-AAA proteases. *Mol. Cell* **35,** 574–585
29. Biter, A. B., Lee, S., Sung, N., and Tsai, F. T. (2012) Structural basis for intersubunit signaling in a protein disaggregating machine. *Proc. Natl. Acad. Sci. U.S.A.* **109,** 12515–12520
30. Hess, H. H., and Derr, J. E. (1975) Assay of inorganic and organic phosphorus in the 0.1–5 nanomole range. *Anal. Biochem.* **63,** 607–613
31. Lanzetta, P. A., Alvarez, L. J., Reinach, P. S., and Candia, O. A. (1979) An improved assay for nanomole amounts of inorganic phosphate. *Anal. Biochem.* **100,** 95–97
32. Tang, W. K., Li, D., Esser, L., and Xia, D. (2009) Purification, crystallization and preliminary X-ray diffraction of disease-related mutants of p97. *Acta Crystallogr. Sect. F Struct. Biol. Cryst. Commun.* **65,** 1166–1170
33. Otwinowski, Z., and Minor, W. (1997) Processing of x-ray diffraction data collected in oscillation mode. *Methods Enzymol.* **276,** 307–326
34. Storoni, L. C., McCoy, A. J., and Read, R. J. (2004) Likelihood-enhanced fast rotation functions. *Acta Crystallogr. D Biol. Crystallogr.* **60,** 432–438
35. Murshudov, G. N., Vagin, A. A., and Dodson, E. J. (1997) Refinement of macromolecular structures by the maximum-likelihood method. *Acta Crystallogr. D Biol. Crystallogr.* **53,** 240–255
36. Collaborative Computational Project, Number 4 (1994) The CCP4 suite. Programs for protein crystallography. *Acta Crystallogr. D Biol. Crystallogr.* **50,** 760–763
37. Emsley, P., and Cowtan, K. (2004) Coot. Model-building tools for molecular graphics. *Acta Crystallogr D Biol. Crystallogr.* **60,** 2126–2132
38. Briggs, L. C., Baldwin, G. S., Miyata, N., Kondo, H., Zhang, X., and Freemont, P. S. (2008) Analysis of nucleotide binding to P97 reveals the properties of a tandem AAA hexameric ATPase. *J. Biol. Chem.* **283,** 13745–13752
39. Tang, W. K., and Xia, D. (2012) Structural and functional deviations in disease-associated p97 mutants. *J. Struct. Biol.* **179,** 83–92
40. Karata, K., Inagawa, T., Wilkinson, A. J., Tatsuta, T., and Ogura, T. (1999) Dissecting the role of a conserved motif (the second region of homology) in the AAA family of ATPases. Site-directed mutagenesis of the ATP-dependent protease FtsH. *J. Biol. Chem.* **274,** 26225–26232
41. Walker, J. E., Saraste, M., Runswick, M. J., and Gay, N. J. (1982) Distantly related sequences in the α- and β-subunits of ATP synthase, myosin, kinases and other ATP-requiring enzymes and a common nucleotide binding fold. *EMBO J.* **1,** 945–951
42. Song, C., Wang, Q., and Li, C. C. (2003) ATPase activity of p97-valosin-containing protein (VCP). D2 mediates the major enzyme activity, and D1

contributes to the heat-induced activity. *J. Biol. Chem.* **278,** 3648–3655
43. Ye, Y., Meyer, H. H., and Rapoport, T. A. (2003) Function of the p97-Ufd1-Npl4 complex in retrotranslocation from the ER to the cytosol. Dual recognition of nonubiquitinated polypeptide segments and polyubiquitin chains. *J. Cell Biol.* **162,** 71–84
44. Meyer, H. H., Kondo, H., and Warren, G. (1998) The p47 co-factor regulates the ATPase activity of the membrane fusion protein, p97. *FEBS Lett.* **437,** 255–257
45. Wang, Q., Song, C., Irizarry, L., Dai, R., Zhang, X., and Li, C. C. (2005) Multifunctional roles of the conserved Arg residues in the second region of homology of p97/valosin-containing protein. *J. Biol. Chem.* **280,** 40515–40523